ACS OMEGA

http://pubs.acs.org/journal/acsodf

Article

Luminescence Temperature Sensing and First Principles Calculation of Photoelectric Properties in C12A7 Co-Doped Eu^{3+} Ions

Yandong Bai, Rui Wang, Yongmei Li,* and Yuemei Li*

Cite This: *ACS Omega* 2023, 8, 15730−15740

Read Online

ACCESS | Metrics & More | Article Recommendations | Supporting Information

ABSTRACT: Developing high-resolution, high-accuracy fluorescent thermometers is challenging. In this study, the optical properties and thermal sensing of Yb-, Tm-, and Eu-co-doped C12A7 (C12A7:Yb/Eu/Tm), with flower-like structure upconversion microparticles, were studied. Eu^{3+} doping induced an approximately 6-fold change in the upconversion luminescence (UCL) output in comparison with C12A7:Yb/Tm microparticles. The maximum relative temperature sensitivity (S) of C12A7:Yb/Eu/Tm reached 3.0% K^{-1}, representing an approximately 5-fold difference compared with the value of C12A7:Yb/Tm. In particular, the multicolor upconversion emission of C12A7:Yb/Eu/Tm can easily change from blue to white UCL with increasing temperature. Moreover, the band structure, total density, and optical coefficient of C12A7:Yb/Eu/Tm were investigated via density functional theory. The total density of O atoms increased in comparison with the total density of pure C12A7, indicating that substitution of Ca^{2+} by Yb/Eu/Tm produced positive vacancies on the cage structure. The optical coefficient of C12A7 was improved by the Yb/Eu/Tm dopant. The thermally regulated multicolor characteristics and thermally coupled energy levels of Tm^{3+} provide "dual adjustment temperature sensing", which is a promising strategy for realizing accurate and effective temperature sensors.

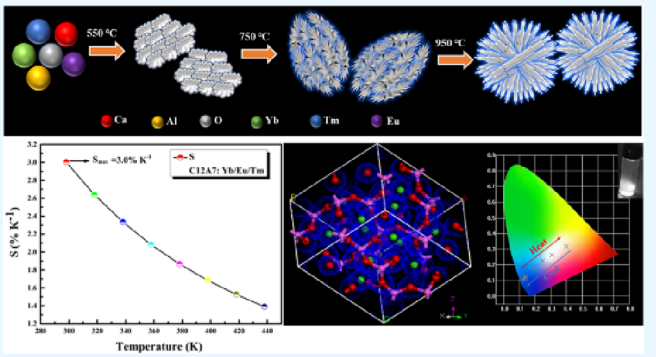

1. INTRODUCTION

Temperature is an important physical parameter in scientific research. As an alternative to traditional thermometers, noncontact temperature sensors have attracted great interest and have application potential in various fields. Noncontact thermometers include the ones based on the temperature dependence of wavelength, intensity, and decay lifetime.[1−3] Optical temperature sensing based on the upconversion luminescence (UCL) intensity ratio of thermally coupled energy levels (TCELs) has received considerable attention due to its high anti-interference and resolution. Temperature can be detected based on the fluorescence intensity ratio (FIR).[4−7] UCL emission is an anti-Stokes process, in which long-wavelength light is absorbed and short-wavelength light is excited.[8,9] Lanthanide ions, such as Er^{3+}, Nd^{3+}, and Tm^{3+}, have high energy levels.[10,11] Two TCELs can be used to achieve a temperature following a Boltzmann distribution.[5,7,12−14]

Eu^{3+} ions have an electron configuration of $4f^7$ orbits, which can tune emission from the blue to red region of the visible spectrum. Eu^{3+} ions show lattice vibration and symmetry, and the lengths of the ligand−Eu^{3+} band make Eu^{3+} ions good candidates for a temperature probe. However, luminescence emission can be influenced by the host lattice.[15,16] Recent studies of thermal effects have focused on oxide hosts due to their high chemical and physical stability.[17−22] The $12CaO·7Al_2O_3$ (C12A7) oxide has a cage structure, which had good insulation performance, wide optical absorption band gap, and good optical transparency. One cage structure is connected with eight adjacent ones in a three-dimensional space, which promotes the optical stability of C12A7.[23,24] The C12A7 crystal due to its close arrangement structure had excellent chemical stability and thermal stability, which realized the precise detection of temperature. The material has potential photoelectric applications due to its good physical and chemical properties.[25−28] However, temperature sensing based on the ratio of monochromatic fluorescence intensity continuously has limited popularity. Temperature sensing based on multicolor fluorescence, instead of intensity, could solve this problem.

In this work, we propose a strategy to enhance UCL and realize the multicolor output via Eu^{3+} doping of C12A7:Yb/Tm upconversion microparticles. The relative sensitivity, based on the intensity ratio of TCELs of Tm^{3+}, was studied at different temperatures. With Eu^{3+} ion doping, the relative

Received: February 28, 2023
Accepted: April 7, 2023
Published: April 19, 2023

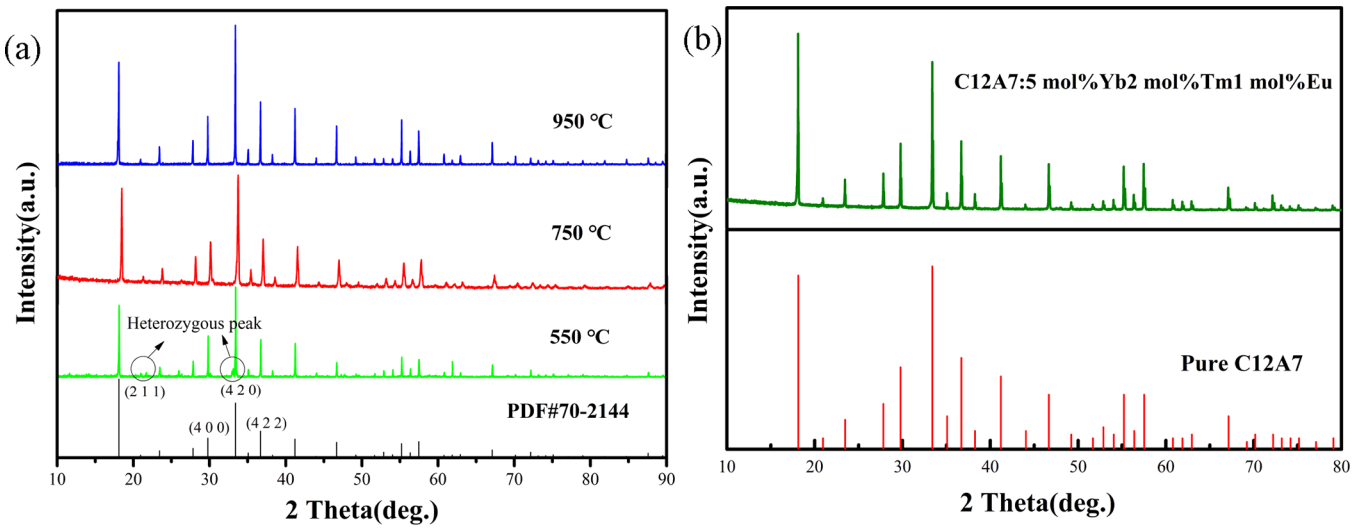

Figure 1. (a) X-ray diffraction patterns of C12A7:Yb/Tm with different annealing temperatures and (b) C12A7:Yb/Eu/Tm microcrystals.

temperature sensitivity (S) of C12A7:Yb/Eu/Tm increases. In addition, the UCL color changes from blue to white with the temperature increase from 298 to 438 K, which enhances temperature sensing and provides highly effective temperature detection. Furthermore, the influence of Yb/Eu/Tm doping on the C12A7 local structure was calculated via density functional theory (DFT). The band structure, total electron density, and optical coefficient were explored for pure C12A7 and C12A7:Yb/Eu/Tm.

2. EXPERIMENTAL SECTION

2.1. Materials. The $12CaO{\cdot}7Al_2O_3$ (C12A7) polycrystals doped with different concentrations of Eu^{3+}, Yb^{3+}, and Tm^{3+} were prepared through the sol−gel method. Raw materials of $Ca(NO_3)_2{\cdot}4H_2O$ (99.99%), $Al(NO_3)_3{\cdot}9H_2O$ (99.99%), $Eu(NO_3)_3{\cdot}5H_2O$ (99.99%), $Tm(NO_3)_3{\cdot}5H_2O$ (99.99%), and $Yb(NO_3)_3{\cdot}5H_2O$ (99.99%) were used in the experiment.

2.2. Synthesis of C12A7:Yb/Eu/Tm. $Ca(NO_3)_2{\cdot}4H_2O$ (12 mmol), $Al(NO_3)_3{\cdot}9H_2O$ (7 mmol), $Eu(NO_3)_3{\cdot}5H_2O$ (0.5−1.5 mol %), $Tm(NO_3)_3{\cdot}5H_2O$ (1−3 mol %), and $Yb(NO_3)_3{\cdot}5H_2O$ (4−6 mol %) were mixed completely in mortars and then added citric acid (20 wt %) and glycol and polyethylene glycol with magnetic stirring at 70 °C for 12 h. The mixture was heated at 90 °C in an oven for 24 h, forming the sol. By annealing temperature (450−950 °C), the C12A7:Yb/Tm and C12A7:Yb/Eu/Tm were obtained.

2.3. Characterization. The UCL spectra were recorded by an SPEX1000M spectrometer with a photomultiplier tube under 980 nm at room temperature. The X-ray diffraction of the C12A7:Yb/Tm and C12A7:Yb/Eu/Tm upconversion materials was recorded by XRD-600 with a speed of 10°/min. The morphology of the as-prepared samples was observed by scanning electron microscopy (SEM). Temperature sensing was measured by a heating platform with an upconversion emission system. The C12A7 and C12A7:Yb/Eu/Tm materials visualizer module was built via Materials Studio 8.0 software. The lattice constant was set as the experimental value adopted in most literatures (a = 11.989 Å), and the space group was $I\overline{4}3d$ (Table S1). The fractional coordinates of each atom in the crystal are as follows.

3. RESULTS AND DISCUSSION

3.1. Structure and Morphology. Yb^{3+}, Tm^{3+}, and Eu^{3+} ion-co-doped $12CaO{\cdot}7Al_2O_3$ (C12A7) microcrystals were synthesized via the sol−gel method. The annealing temperature had an important influence on the structure and UCL emission of the materials. The structures of C12A7:Yb/Tm microcrystals with different annealing temperatures were confirmed by X-ray diffraction pattern analysis (Figure 1a). Heterozygous diffraction peaks at 22.1, 25.5, and 32.8° were observed with an annealing temperature of 550 °C, which were heterogeneous peaks in the mixture of CaO and Al_2O_3. These results indicated that the crystallinity and purity of samples were not enough at 550 °C. Eu^{3+}/Tm^{3+} (Re^{3+}) ion-doped samples formed a complex of ReO_6 with optical activity, which realized UCL. Re^{3+} was located in the center in the ReO_6. Owing to the different bond lengths between Re^{3+} and the surrounding O atoms, ReO_6 formed a C_{4v} symmetric point group. On the contrary, the point group with high symmetry cannot make Re^{3+} have a UCL effect. In the C12A7 system, Ca coordinates with the surrounding six O atoms formed CaO_6, which had three different Ca−O bond lengths. The optically active ReO_6 complex formed with replacing the position of Ca^{2+} in Re^{3+} ion-doped C12A7, which made Re^{3+} generate UCL. Therefore, substitution of Ca^{2+} in C12A7 doped with Yb/Eu/Tm was carried out, which suggested that the synthesis of C12A7:Yb/Eu/Tm required a higher temperature than 550 °C. The X-ray diffraction pattern had no second diffraction peaks, in correspondence with JCPDS file no. 70-2144, and the intensity of the diffraction peaks increased with temperature from 750 to 950 °C. As shown in Figure 1b, the diffraction peaks of the C12A7:Yb/Eu/Tm matched well with the (2 1 1), (4 0 0), (4 2 0), and (4 2 2) planes of pure C12A7, respectively. No other phase was detected with the Yb, Tm, or Eu dopant, indicating that Yb/Tm/Eu ions dissolved in the C12A7 host matrix by substituting for the Ca^{2+} ion.

To obtain additional structural information, SEM images were analyzed to determine the structure of C12A7:Yb/Eu/Tm. With an annealing temperature of 550 °C, the samples had a spherical structure in SEM images (Figure 2b), and the average size of the samples was about 150 nm (Figure 2e). When the annealing temperature was increased to 750 °C, as demonstrated in Figure 2c,f, a high-quality flower-like structure

https://doi.org/10.1021/acsomega.3c01372
ACS Omega 2023, 8, 15730−15740

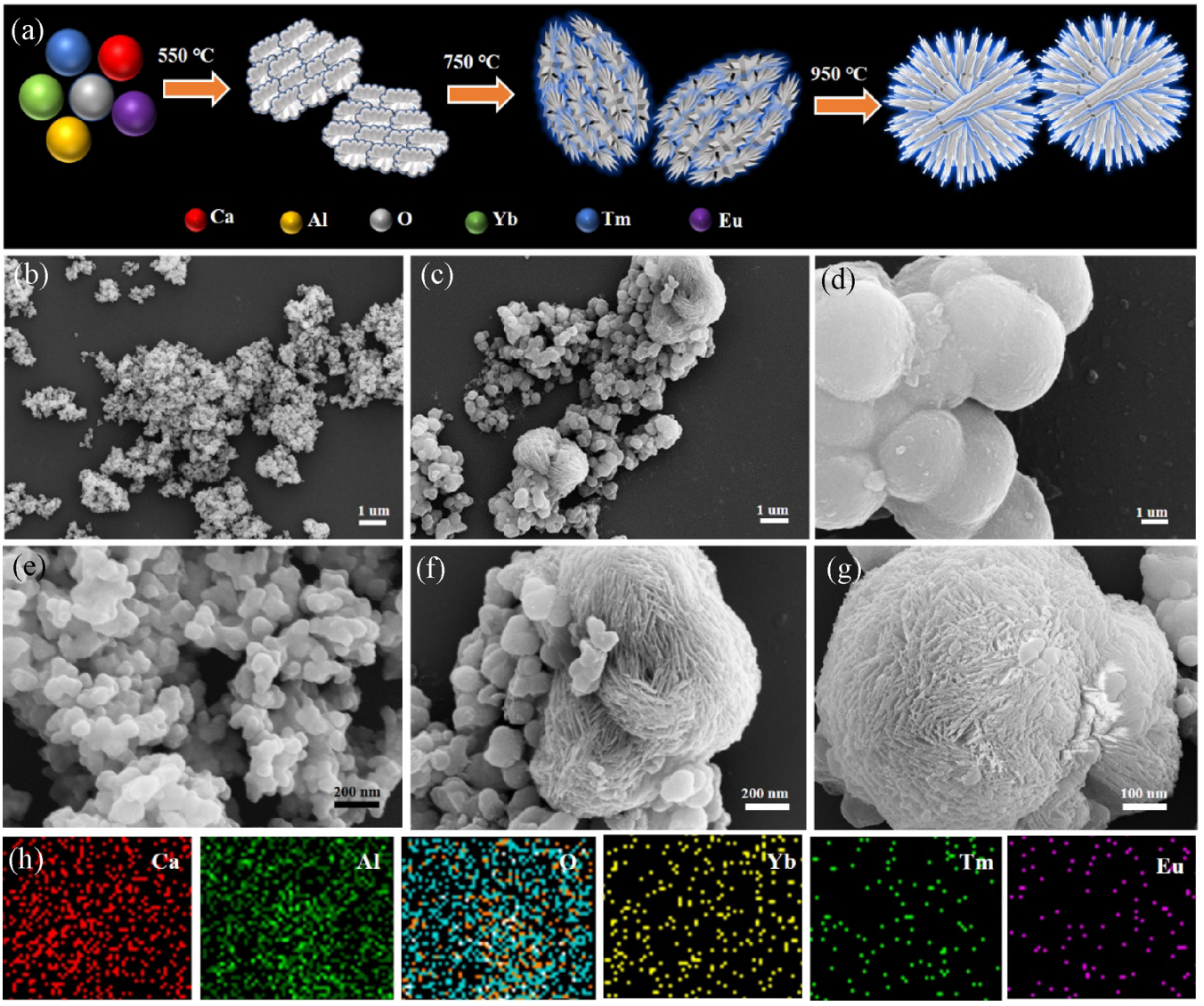

Figure 2. (a) Schematic illustration of the morphology evolution mechanism of C12A7:Yb/Eu/Tm microcrystals via increasing the annealing temperature from 550 to 950 °C. SEM images of the C12A7:Yb/Eu/Tm polycrystal with (b) and (e) 550 °C, (c) and (f) 750 °C, and (d) and (g) 950 °C. (h) EDS mapping of the C12A7:Yb/Eu/Tm polycrystal; the red, green, blue, yellow, dark green, and purple colors of EDS mappings were respectively Ca, Al, O, Yb, Tm, and Eu elements.

of C12A7:Yb/Eu/Tm was observed. The average size of C12A7:Yb/Eu/Tm microcrystals increased with annealing temperature. As shown in Figure 2d,g, a uniform spherical structure was observed in the annealing temperature range of 750 to 950 °C. As demonstrated in Figure 2a, a flower-like structure was achieved and the average size increased with increasing annealing temperature. Moreover, energy-dispersive spectrometer (EDS) mapping analysis (Figure 2d) revealed the presence of Ca, Al, O, Yb, Tm, and Eu, demonstrating the successful preparation of C12A7:Yb/Eu/Tm microcrystals (Figure 2h).

3.2. UCL Property. To investigate how different concentrations of lanthanide ion dopants influence the UCL of samples, we synthesized C12A7:Yb/Tm and C12A7:Yb/Eu/Tm co-doped with different concentrations of Yb, Tm, and Eu ions. As presented in Figure 3a, the C12A7:Yb/Tm polycrystal emitted blue UCL at 475 nm, red UCL at 651 nm, and NIR UCL at 800 nm, which was attributed to the $^1G_4 \rightarrow {}^3H_6$, $^1G_4 \rightarrow {}^3F_4$, and $^3H_4 \rightarrow {}^3H_6$ transitions of Tm^{3+} ions, respectively. The concentration of Tm^{3+} ions remained at 2 mol %. In the case of C12A7:Yb/Tm, the UCL emission intensity first increased and then decreased with increasing Yb^{3+} concentration from 4 to 6 mol %. The UCL intensity of samples reached a maximum value at 5 mol % Yb^{3+}, representing an approximately 6-fold increase compared with the value of C12A7:Yb/Tm with 4 mol % Yb^{3+}. These results proved that the concentration of Yb^{3+} ions for sensitization needs to be controlled. Decreased UCL emission at higher sensitizer concentrations originated from the quenching of Yb^{3+} ions by surrounding solvents. The amount of Tm^{3+}, as a luminescence center ion, played a key role in UCL emission. As shown in Figure 3b, the UCL emission spectra of C12A7:Yb/Tm with different amounts of Tm^{3+} ions were characterized at 5 mol % Yb^{3+}, and the UCL intensity of samples showed an initial increase and then a decrease with increasing Tm^{3+} concentration from 1 to 3 mol %. The intensity of samples at 2 mol % Tm^{3+} was enhanced about 4-fold compared with the samples at 1 mol % Tm. A low

https://doi.org/10.1021/acsomega.3c01372
ACS Omega 2023, 8, 15730−15740

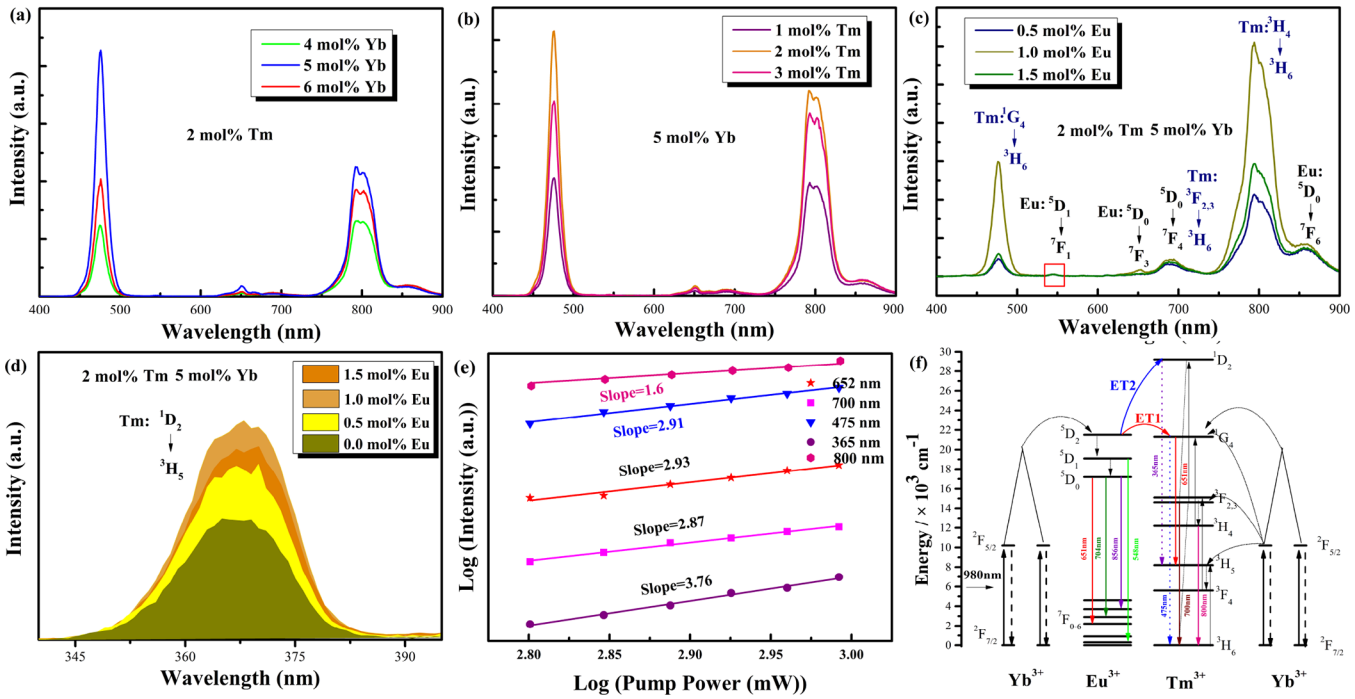

Figure 3. UCL emission spectra of C12A7:Yb/Tm with different (a) Yb^{3+} ions (2 mol % Tm^{3+}) and (b) Tm^{3+} ions (5 mol % Yb^{3+}). (c) UCL emission spectra of C12A7:Yb/Eu/Tm with different Eu^{3+} ions (2 mol % Tm^{3+} and 5 mol % Yb^{3+}). (d) UV UCL emission spectra of C12A7:Yb/Eu/Tm with different Eu^{3+} ions. (e) Corresponding Log (intensity)−Log (pump power) curve of C12A7:Yb/Eu/Tm. (f) Proposed energy transfer mechanisms under the irradiation of a 980 nm laser.

concentration of Tm^{3+} ions resulted in low energy efficiency, whereas a high amount of Tm^{3+} ions led to energy back-transfer. Eu^{3+} ions can be used as coupling ions to enhance the transfer efficiency of C12A7:Yb/Tm. To assess the influence of Eu^{3+} doping on the UCL emission of C12A7:Yb/Eu/Tm microcrystals, the UCL properties of samples with different amounts of Eu^{3+} were measured, as shown in Figure 3c. Different from the UCL emission of C12A7:Yb/Eu/Tm, UCL at wavelengths of 548 nm (green), 651 nm (red), 704 nm (red), and 856 nm (NIR) was achieved, which corresponded to the $^5D_1 \rightarrow {}^7F_1$, $^5D_0 \rightarrow {}^7F_3$, $^5D_0 \rightarrow {}^7F_4$, and $^5D_0 \rightarrow {}^7F_5$ transitions of Eu^{3+} ions, respectively. The red UCL emission (651 and 704 nm) of Eu^{3+} overlapped with the UCL of Tm^{3+}, which enhanced the intensity of red UCL emission. The red UCL intensity of C12A7:Yb/Eu/Tm was increased approximately 6-fold in comparison with that of C12A7:Yb/Tm. It is worth noting that the ultraviolet (UV) UCL intensity of C12A7:Yb/Eu/Tm was significantly enhanced at 365 nm, attributable to the $^1D_2 \rightarrow {}^3H_5$ transition of Eu^{3+} ions (Figure 3d). When the Eu ion concentration was 1 mol %, the intensity of the UV UCL emission reached its maximum at 2 mol % Tm^{3+} and 5 mol % Yb^{3+}. These results proved that Eu^{3+} doping increased the UCL intensity of the samples. As shown in Figure 3f, the UCL mechanism of C12A7:Yb/Eu/Tm was analyzed. Under 980 nm laser irradiation, the UCL emission of Tm^{3+} increased as a result of Eu^{3+} doping. Yb^{3+} ions, as a sensitizer, continuously absorbed energy from the 980 nm photons of the laser excitation and transferred it to Eu^{3+} ions simultaneously via energy transfer (ET). The Eu^{3+} ions absorbed the energy, which led to $^5D_1 \rightarrow {}^7F_1$, $^5D_2 \rightarrow {}^7F_3$, $^5D_2 \rightarrow {}^7F_4$, and $^5D_2 \rightarrow {}^7F_5$ transitions of the Eu^{3+} ions. The Eu^{3+} ions transferred energy to Tm^{3+} though ET1 and ET2 processes. Two processes were proposed based on analyses of the spectra:

$$\text{ET1: } {}^5D_2(Eu^{3+}) + {}^3H_6(Tm^{3+}) \rightarrow {}^7F_0(Eu^{3+}) + {}^1G_4(Tm^{3+})$$

$$\text{ET2: } {}^5D_2(Eu^{3+}) + {}^3H_5(Tm^{3+}) \rightarrow {}^7F_0(Eu^{3+}) + {}^1D_2(Tm^{3+})$$

The $^1D_2$ and $^1G_4$ levels of Tm^{3+} absorbed energy from Eu^{3+} ions, relaxing to the $^3H_5$ and $^3H_6$ levels, respectively, and exciting the 365, 651, and 475 nm UCL. Additionally, the $^1G_4$ and $^3F_{2,3}$ states of Tm^{3+} absorbed energy from Yb^{3+} and relaxed to the $^3H_5$ and $^3H_6$ levels of Tm^{3+}. The intensity of the UCL emission and pump power followed (eq 1):

$$I_f \propto p^n \quad (1)$$

where I_f is the fluorescence intensity, P is the pump laser power, and n is the number of photons required in the UC process. As illustrated in Figure 3e, the slopes of C12A7:Yb/Eu/Tm UCL at 365, 475, 651, 700, and 800 nm increased to 3.76, 2.91, 2.93, 2.87, and 1.61, respectively. These results proved that UV UCL, blue and red UCL, and NIR UCL were three-, four-, and two-photon processes, which were typically different from the previous study. In addition, the green, red, and NIR (856 nm) of C12A7:Yb/Eu/Tm increased compared with that of C12A7:Yb/Eu (Figure S1), indicating that Tm^{3+} played an important role in the ET process. The Eu^{3+} gain energy from Yb^{3+} via the cooperative upconversion process. Tm^{3+} as another "sensitizer" (for Eu^{3+}) transferred energy to Eu^{3+} ions by ET. To further explore the UCL properties of Yb/Tm/Eu/C12A7 polycrystals with Eu^{3+} ion doping, the luminescence decay lifetime of the intermediate level $^1D_5$ of Eu^{3+} is shown in Figure S2. The luminescence decay lifetime can be used by eqs 2 and 3:

https://doi.org/10.1021/acsomega.3c01372
ACS Omega 2023, 8, 15730−15740

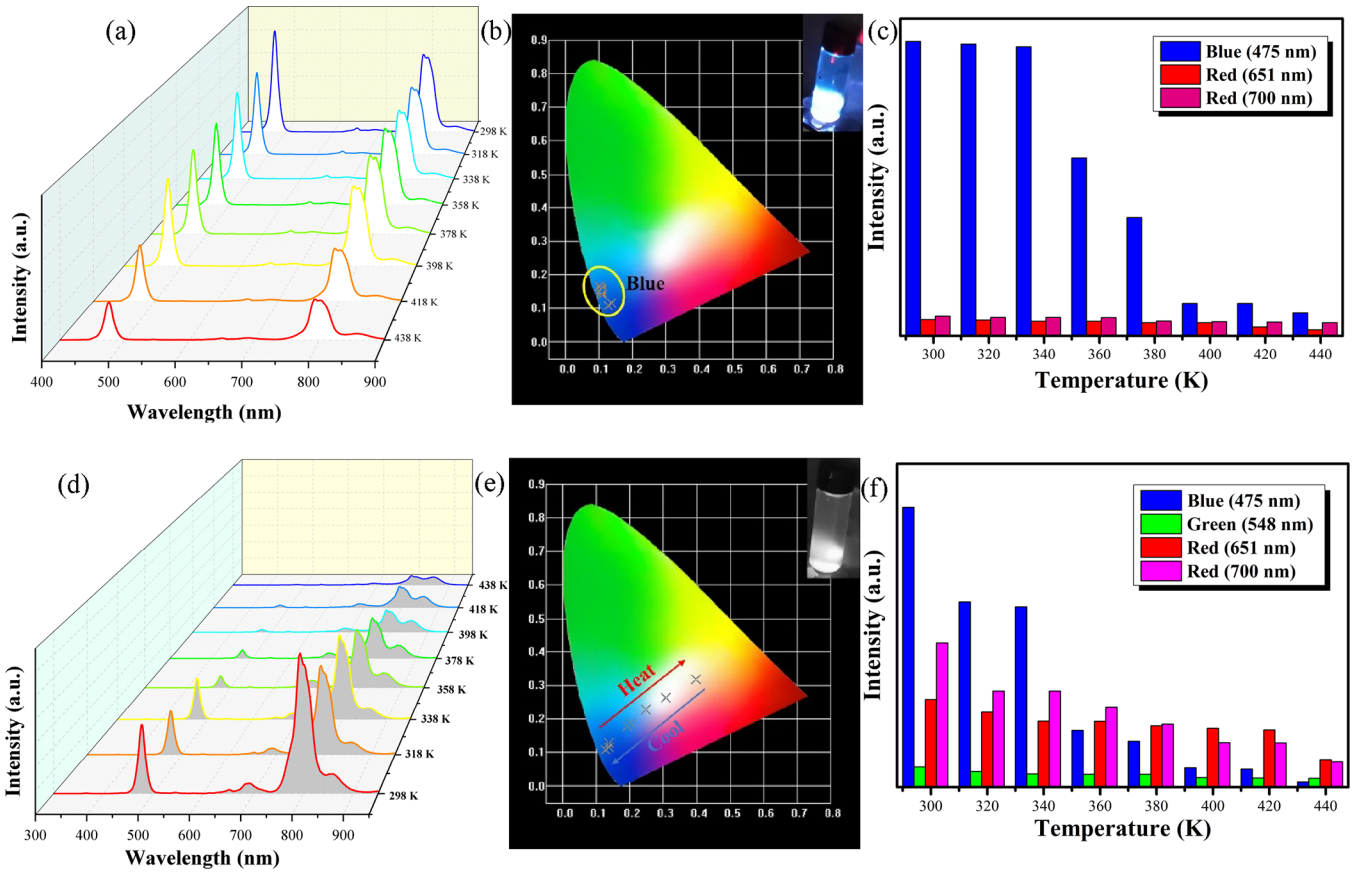

Figure 4. (a) Upconversion spectra of C12A7:Yb/Tm with the increase from 298 to 438 K. (b) CIE analysis at different temperatures in Yb/Tm/C12A7 with the increase from 298 to 438 K. The inset was the UCL photo of Yb/Tm/C12A7 at 438 K. (c) Intensities of blue and red UCL of C12A7:Yb/Tm with different temperatures. (d) Upconversion spectra of C12A7:Yb/Eu/Tm with the increase from 298 to 438 K. (e) CIE analysis at different temperatures in C12A7:Yb/Eu/Tm with the increase from 298 to 438 K. The inset was the UCL photo of C12A7:Yb/Eu/Tm at 438 K. (f) Intensities of blue, green, and red UCL of C12A7:Yb/Eu/Tm with different temperatures.

$$I(t) = I_0 + A_s e^{-\tau/\tau_s} + A_f e^{-\tau/\tau_f} \quad (2)$$

$$\tau = \frac{A_s\tau_s^2 + A_f\tau_f^2}{A_s\tau_s + A_f\tau_f} \quad (3)$$

where I_0 was the intensity of fluorescence in the back; A_f and A_s were the weighting factor of fast fluorescence lifetime and weighting factor of slow fluorescence lifetime, respectively; and τ_f and τ_s were the fast and slow fluorescence lifetimes, respectively. The decay lifetime of $^1D_5$ of Eu^{3+} for Tm/C12A7 was 687 μs. These results implied that the metastable state of Eu^{3+} had a long energy level decay lifetime, which was benefited to improve the UCL intensity.

3.3. Temperature-Sensing Property. To study the effect of Eu^{3+} doping on the optical properties of samples further, the UCL emissions of C12A7:Yb/Tm and C12A7:Yb/Eu/Tm, with increasing temperature from 298 to 438 K, were explored with a power density of 350 mW. As shown in Figure 4a,d, the UCL intensity of C12A7:Yb/Tm and C12A7:Yb/Eu/Tm decreased gradually with increasing temperature because the thermal effect increased the fluorescence quenching effect. In addition, the green UCL was obtained via doping of Eu^{3+} ions (Figure 4f). As illustrated in Figure 4c,f, the intensity of blue UCL decreased significantly with an increase of temperature from 298 to 438 K, while the intensities of red and green UCL showed a slight decrease. These results implied that the color changed with temperature. To verify the multicolor changes further, the CIE color space values of samples at different temperatures were calculated via eqs 4−9:

$$x = \frac{X}{X + Y + Z} \quad (4)$$

$$y = \frac{Y}{X + Y + Z} \quad (5)$$

$$z = \frac{Z}{X + Y + Z} \quad (6)$$

$$X = \int_{400}^{700} p(\lambda)x'(\lambda)d\lambda \quad (7)$$

$$Y = \int_{400}^{700} p(\lambda)y'(\lambda)d\lambda \quad (8)$$

$$Z = \int_{400}^{700} p(\lambda)z'(\lambda)d\lambda \quad (9)$$

In the above, $p(\lambda)$ is the emission intensity at the λ band, and $x'(\lambda)$, $y'(\lambda)$, and $z'(\lambda)$ are the respective color partition functions. The CIE coordinates of Yb/Tm/C12A7 changed from (0.1919, 0.1771) to (0.1376, 0.1142) with the temperature change from 298 to 438 K under 980 nm excitation. The triangle in the 1931 CIE chromaticity diagram is shown in Figure 4b. The UCL emission color of C12A7:Yb/Tm remained blue with the temperature increase, as shown in

https://doi.org/10.1021/acsomega.3c01372
ACS Omega 2023, 8, 15730−15740

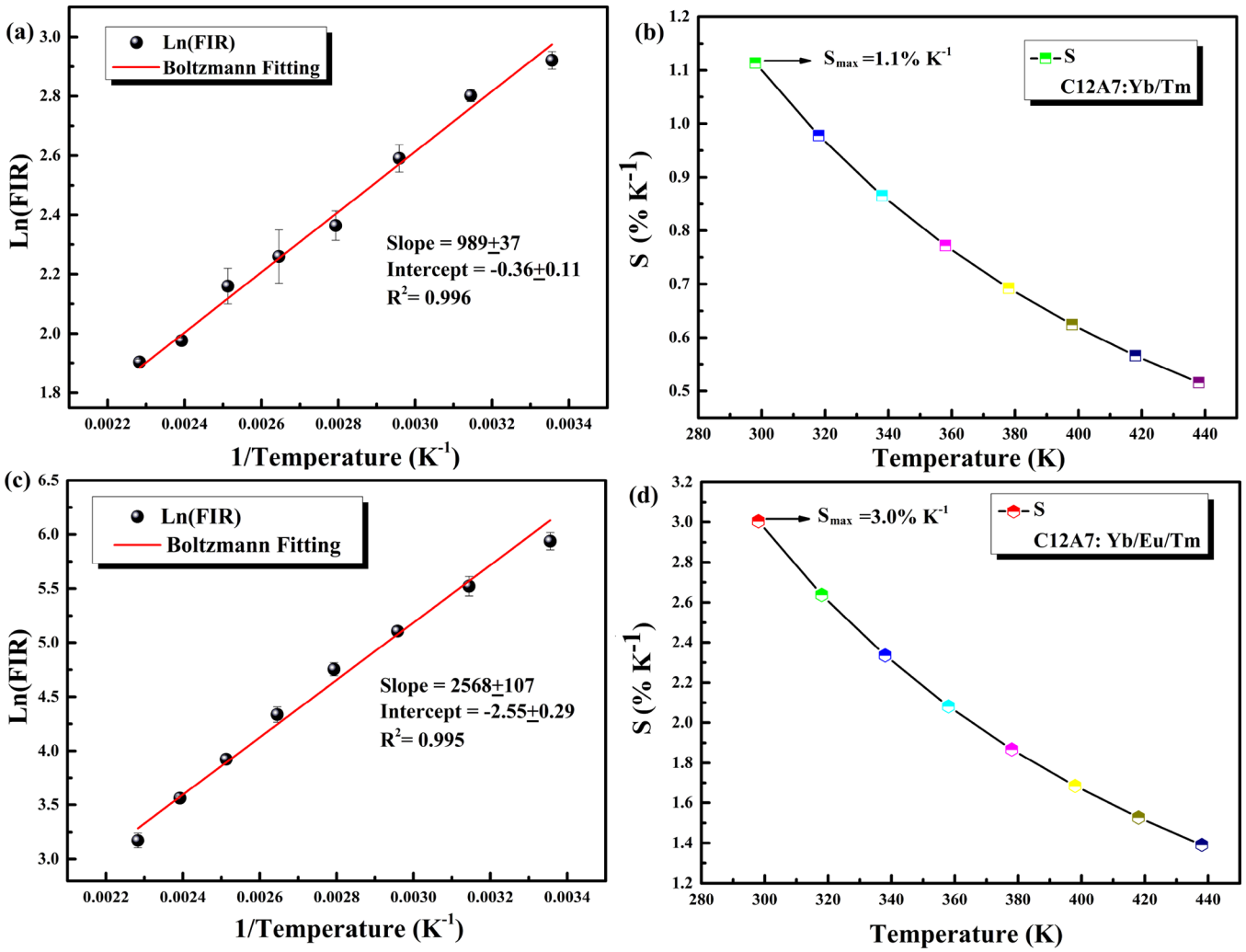

Figure 5. (a) Plot of the FIR ($I_{700/800}$) as a function of temperature in C12A7:Yb/Tm. (b) Variation of S for C12A7:Yb/Tm with increasing temperatures. (c) Plot of the FIR ($I_{700/800}$) as a function of temperature in C12A7:Yb/Eu/Tm. (d) Variation of S for C12A7:Yb/Eu/Tm with increasing temperatures.

the inset of the photograph in Figure 4b. The CIE coordinates of C12A7:Yb/Eu/Tm changed from (0.1276, 0.1078) to (0.3987, 0.3181) with an increase of temperature. The color of C12A7:Yb/Eu/Tm changed from blue to white to yellow with higher temperatures, indicating that multicolor behavior can be realized via temperature adjustment (Figure 4e). The white UCL emission of C12A7:Yb/Eu/Tm is shown in the inset of Figure 4e. As a result of the Eu^{3+} ion dopant, the UCL color of the sample showed a temperature-dependent variation, changing from blue to white light with heating to 438 K and recovering to blue light emission with cooling to 298 K.

The temperature-sensing capabilities based on the ratio between 700 and 800 nm were measured for C12A7:Yb/Tm and C12A7:Yb/Eu/Tm in the range of 298 to 438 K. The $^3F_{2,3}$ and $^3H_4$ states of Tm^{3+} ions were TCELs, which followed a Boltzmann fitting, and these levels of Tm^{3+} ions were attributed to wavelengths of 700 and 800 nm, respectively. The ratio of 700 and 800 nm (i.e., the FIR) can be used in eq 10:

$$\mathrm{FIR} = \frac{I_i}{I_j} = A\exp\left(-\frac{\Delta E}{k_B T}\right) + B \tag{10}$$

where I_j and I_i are the fluorescence intensity of the low TCEL and fluorescence intensity of the high TCEL, respectively. ΔE and k_B represent the energy band gap between the two TCELs and the Boltzmann constant, respectively. Equation 11 follows eq 10:

$$\ln(\mathrm{FIR}) = \ln\left(\frac{I_i}{I_j}\right) = -\frac{\Delta E}{k_B T} \tag{11}$$

Figure 5a illustrates the relation between ln(FIR) and the temperature of C12A7:Yb/Tm, with a slope of $\Delta E/k_B$ (989). The $\Delta E/k_B$ of C12A7:Yb/Eu/Tm was 2568 (Figure 5c), which was larger than the slope of C12A7:Yb/Tm. The sensitivity (S) can be determined via eq 12:

$$S = \frac{1}{\mathrm{FIR}}\left|\mathrm{d}\frac{\mathrm{FIR}}{\mathrm{d}T}\right| \times 100\% = \frac{\Delta E}{k_B T^2} \times 100\% \tag{12}$$

As shown in Figure 5b,d, the S value increased gradually with temperature from 298 to 438 K for C12A7:Yb/Tm and C12A7:Yb/Eu/Tm. According to eq 10, the maximum values of S of C12A7:Yb/Tm and C12A7:Yb/Eu/Tm reached 1.1 and 3.0% K^{-1}, respectively. Eu^{3+} ion doping decreased the crystal field symmetry of samples, which increased the effect of

https://doi.org/10.1021/acsomega.3c01372
ACS Omega 2023, 8, 15730−15740

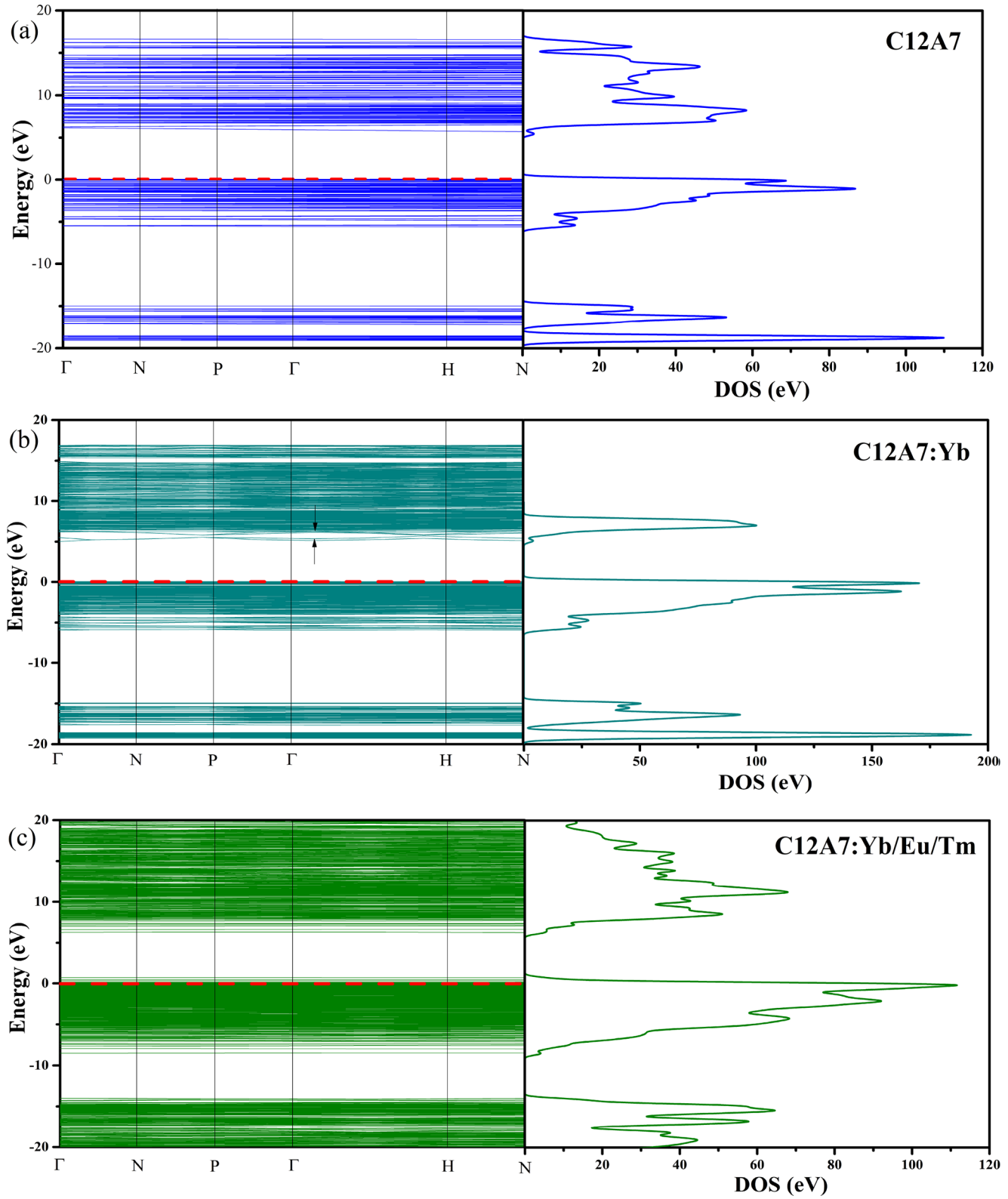

Figure 6. Band structures of the crystals: (a) band structure of pure C12A7, (b) band structure of C12A7:Yb, and (c) band structure of C12A7:Yb/Eu/Tm.

the crystal field on Tm^{3+} ions.[32−36] This result led to a larger energy level gap between 700 and 800 nm. This crystal field also broadened the transition barrier, making the emission intensity enhance. The modulation of the crystal field on Tm became stronger. The 800 nm fluorescence intensity of C12A7:Yb/Eu/Tm with Eu^{3+} doping decreased faster than that of C12A7:Yb/Tm. Moreover, the decay lifetime of the band at 800 nm increased from 546 to 760 μs with doping of Eu^{3+} ions, which indicates that photons at an energy level of 800 nm were easier to lay out to the corresponding energy

https://doi.org/10.1021/acsomega.3c01372
ACS Omega 2023, 8, 15730−15740

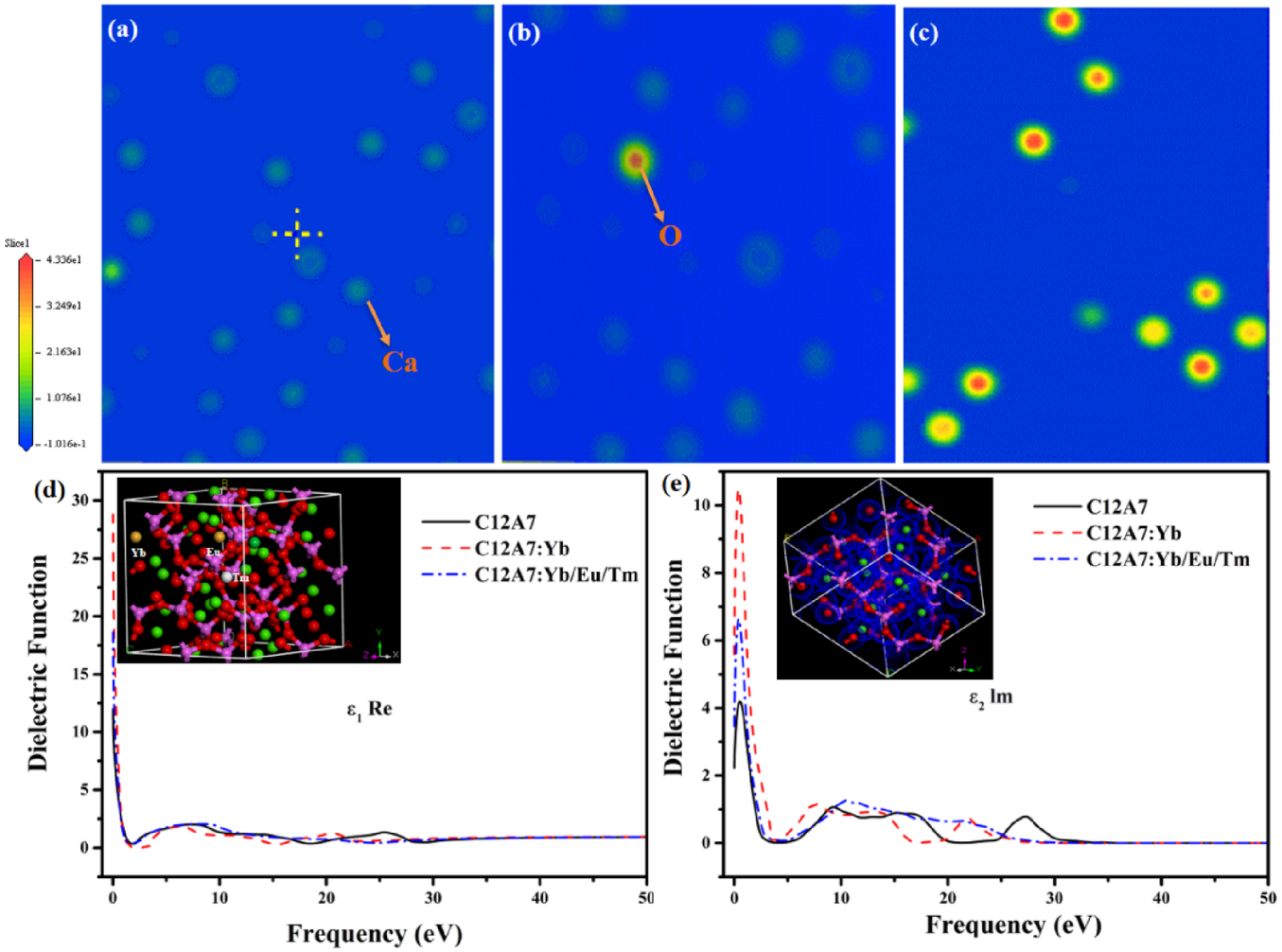

Figure 7. (a) Total electron density of pure C12A7, (b) Yb of 5 mol % doped C12A7, and (c) Yb/Eu/Tm-doped C12A7. (d) Real part of the dielectric function ε_1 of polycrystalline with Yb and Eu/Tm doping; the inset was the model of C12A7:Yb/Eu/Tm. (e) Imaginary part of the dielectric function ε_2 of polycrystalline with Yb and Eu/Tm doping; the inset was the potential electron density of C12A7:Yb/Eu/Tm.

level of 700 nm (Figure S3). The change lnFIR value of C12A7:Yb/Eu/Tm increased compared with that of C12A7:Yb/Tm. The *S* of C12A7:Yb/Eu/Tm was high in comparison with the values of other rare earth-doped oxide materials (Table S2). These results prove that C12A7:Yb/Eu/Tm not only has a high *S* but also realizes a color change with different temperatures, indicating application potential for temperature detection.

3.4. First Principles Calculation of Photoelectric Properties. The calculated band structures of pure C12A7 and C12A7:Yb/Eu/Tm are shown in Figure 6. The energy band gap of pure C12A7 was about 5.89 eV (Figure 6a). The C12A7:Yb and C12A7:Yb/Eu/Tm had indirect energy band gaps of about 5.21 and 5.20 eV, respectively (Figure 6b,c). The decrease of the energy band gap in C12A7 indicated that Yb/Eu/Tm doping enhanced its photoelectric properties. In the range of about 5.2−20 eV above the Fermi level (EF), there was a cage conduction band (CCB), which corresponded to cage cavities of C12A7 without free oxygen ions. When Yb/Eu/Tm was co-doped in the Ca^{2+} site, the number of unoccupied CCB cavities increased compared with the value of pure C12A7, suggesting that the O^{2-} ions decreased and an extra electron was delocalized in comparison to pure C12A7. When there was O^{2-} charge compensation, the energy band corresponding to the p orbital of free oxygen ions disappeared. It was obvious that degeneracy of the energy band appeared in the conduction band of the cage. The lattice interaction with the oxygen ion was removed by the free oxygen ion in the cage. The lattice deformation caused by the strong interaction between the two groups, which formed the energy band due to the lattice deformation, decreased. The degeneracy eliminated at some *k* points was restored. These results proved that Yb/Eu/Tm-co-doped C12A7 has enhanced photoelectric properties in comparison to pure C12A7.

The calculated total electron density of C12A7:Yb/Eu/Tm is illustrated in Figure 7. The electron density of the O atom, due to its high energy, shows red in the electronic map. The electron density of the Ca atom, which donated an electron to O, presents as yellow. The Yb/Eu/Tm-doped C12A7 replaced the Ca position (inset of Figure 7d). As illustrated in Figure 7a−c, the total electron density of pure C12A7 presented a yellow-green color, and the total electron density of Yb/Eu/Tm-doped C12A7 appeared yellow and red, which indicated that the electron population of the O atom increased. The transition from Ca to O was enhanced in the Yb/Eu/Tm-doped C12A7 in comparison with that of pure C12A7, suggesting that the electron charge density of the sample surface increased in the C12A7 host via Yb/Eu/Tm

https://doi.org/10.1021/acsomega.3c01372
ACS Omega 2023, 8, 15730−15740

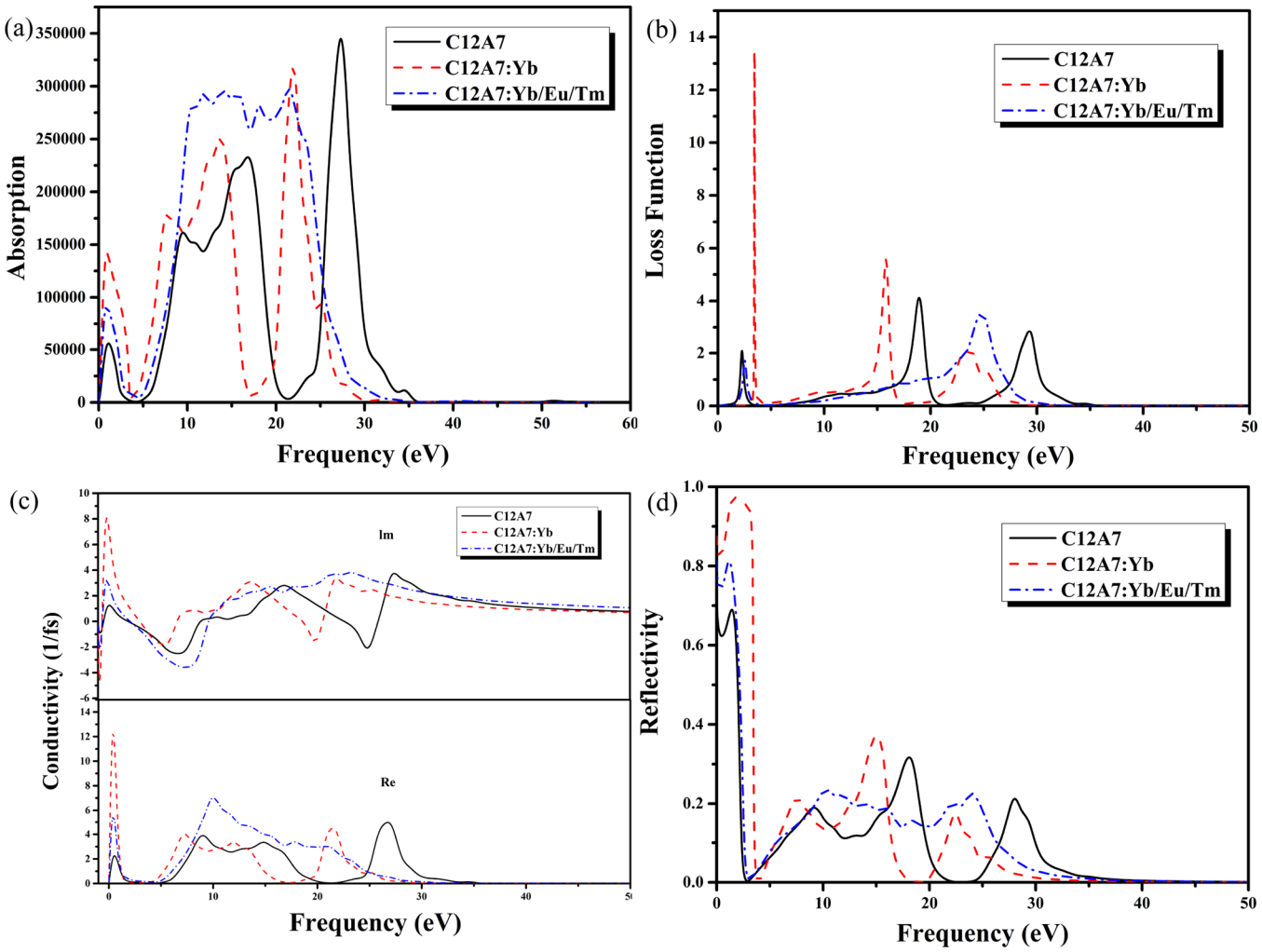

Figure 8. (a) Absorption coefficient of C12A7, C12A7:Yb, and C12A7:Yb/Eu/Tm. (b) Loss function of C12A7, C12A7:Yb, and C12A7:Yb/Eu/Tm. (c) Conductivity of C12A7, C12A7:Yb, and C12A7:Yb/Eu/Tm. (d) Reflectivity of C12A7, C12A7:Yb, and C12A7:Yb/Eu/Tm.

substitution of the Ca atom. The substitution of Ca^{2+} by Yb^{3+}/Eu^{3+}/Tm^{3+} required O^{2-} ions for charge compensation. The replacement of Ca^{2+} produced positive vacancies on the surface for charge balance and generation of transient electric dipoles, with the positive poles pointing outward. Increasing the potential electron density with Yb/Eu/Tm-co-doped C12A7 changed the lattice and atomic distance between Ca and O through the Yb/Eu/Tm dopant (inset of Figure 7e). To explore the electronic structure of the polycrystalline material, the real (ε_1) and imaginary (ε_2) parts of the frequency based on the dielectric function were calculated, as shown in Figure 7d,e and Figure S4. The ε_2 peaks of pure C12A7 at 1, 9, and 27 eV, which originated from transitions from the O f to Ca s, O p to Ca s, and O p to Ca d orbitals, respectively, were observed. For the Yb/Eu/Tm-doped C12A7, the peaks shifted toward the lower energy, which was related to the top of the valence band with dominant contributions from O p and Ca d. The C12A7:Eu and C12A7:Yb/Eu/Tm ratio of ε_1 and ε_2 increased, suggesting that the static dielectric function was enhanced (Figure 7d). With Eu- and Yb/Eu/Tm (Re^{3+})-doping C12A7, the fewer number of peaks proved that there was almost no split in Ca d orbitals, maybe due to the potassium, which more easily loses electrons than Al. These results proved that Re^{3+} ions occupy the position of Ca ions, and UCL center EuO_6 can form. These results indicated that Yb/Eu/Tm-co-doped C12A7 has improved optical properties.

To further explore the optical properties of C12A7, C12A7:Yb, C12A7:Eu, and C12A7:Yb/Eu/Tm, the absorption coefficient, loss function, conductivity, and reflectivity were calculated. As shown in Figure 8, the diffraction peak of absorption, loss function, conductivity, and reflectivity of Yb/Eu/Tm-co-doped C12A7 moved from high to low energy, indicating the occurrence of the Yb/Eu/Tm 4f orbital electron transition. The absorption coefficient and loss function intensities of C12A7:Yb, C12A7:Eu, and C12A7:Yb/Eu/Tm decreased in comparison with the values of C12A7, indicating enhanced photorefractive properties of C12A7 (Figure 8a,b and Figure S5). Conductivity is related to the electric dipole transition between the unoccupied and occupied conditions. The conductivity peak and reflectivity of C12A7:Yb, C12A7:Eu, and C12A7:Yb/Eu/Tm moved to low energy, indicating that the imaginary part of the dielectric function at plasma resonance had an effect on the depth of the plasma minimum with Yb/Eu/Tm ion doping (Figure 8c,d). The loss function peaks of the Re-doped C12A7 crystals were shifted in the lower-energy direction, with the heights decreasing with Re ion doping, which can be recognized by an improvement in the optical properties. These results suggest that the optical

https://doi.org/10.1021/acsomega.3c01372
ACS Omega 2023, 8, 15730−15740

coefficient of C12A7:Yb, C12A7:Eu and C12A7:Yb/Eu/Tm improved in comparison with the coefficient of C12A7.

4. CONCLUSIONS

In summary, we prepared C12A7:Yb/Tm and C12A7:Yb/Eu/Tm microcrystals and realized multicolor UCL emission via doping of Eu^{3+} ions. Based on the intensity ratio of the TCELs of Tm^{3+} ions, the S of C12A7:Yb/Eu/Tm was 3.0% K^{-1}. The UCL color of C12A7:Yb/Eu/Tm changed from blue to white to yellow with heating from 298 to 438 K and could be recovered with cooling. First principles calculation was used to analyze the structure and photoelectric properties of Yb/Eu/Tm-doped C12A7. The optical coefficient of C12A7:Yb/Eu/Tm was improved in comparison with the value of pure C12A7. Therefore, C12A7:Yb/Eu/Tm microcrystals can realize high-efficiency temperature detection through Eu^{3+} ion doping and have potential applications in temperature sensors.

■ ASSOCIATED CONTENT

Data Availability Statement

The data that support the findings of this study are available from the corresponding author, Yuemei Li, upon reasonable request.

Supporting Information

The Supporting Information is available free of charge at https://pubs.acs.org/doi/10.1021/acsomega.3c01372.

Fractional coordinates of each atom; upconversion luminescent spectra of C12A7:Yb/Eu with different Eu ions; luminescence decay lifetime of $^1D_5$ of Eu in the Yb/Tm/Eu/C12A7 system; luminescence decay lifetime of Yb/Tm/C12A7 with 800 nm; luminescence decay lifetime of Yb/Eu/Tm/C12A7 with 800 nm; real part of the dielectric function ε_1 of polycrystalline with Eu-doping C12A7; absorption coefficient of C12A7:Eu; conductivity of C12A7:Eu; reflectivity of C12A7:Eu; loss function of C12A7:Eu; imaginary part of the dielectric function ε_2 of polycrystalline with Eu-doping C12A7; and maximum relative sensitivity (S_r) of some typical rare earth-doped oxide upconversion materials (PDF)

■ AUTHOR INFORMATION

Corresponding Authors

Yongmei Li − *NHC Key Laboratory of Hormones and Development, Tianjin Key Laboratory of Metabolic Diseases, Chu Hsien-I Memorial Hospital & Tianjin Institute of Endocrinology, Tianjin Medical University, Tianjin 300134, China;* orcid.org/0000-0003-1808-6060; Email: liyongmei0811@sina.com

Yuemei Li − *Xiamen Key Laboratory of Cardiovascular Disease, Xiamen Cardiovascular Hospital of Xiamen University, School of Medicine, Xiamen University, Xiamen 361012, China;* orcid.org/0000-0001-5691-845X; Email: 972491839@qq.com

Authors

Yandong Bai − *Tianjin Union Medical Center, Tianjin 300121, China;* orcid.org/0000-0001-7241-9626

Rui Wang − *School of Chemistry and Chemical Engineering, Harbin Institute of Technology, Harbin, Heilongjiang 150001, China;* orcid.org/0000-0002-1964-4776

Complete contact information is available at: https://pubs.acs.org/10.1021/acsomega.3c01372

Notes

The authors declare no competing financial interest.

■ ACKNOWLEDGMENTS

This work was financially supported by the National Natural Science Foundation of China (no. 12104378) and the Xiamen Medical and Health Guidance Project (no. 3502Z20209145). The project is funded by the Xiamen Cardiovascular Hospital, Xiamen University. The software for DFT calculations was from the High Performance Computing Center of Xiamen University.

■ REFERENCES

(1) Shang, Y.; Han, Q.; Hao, S.; Chen, T.; Zhu, Y.; Wang, Z.; Yang, C. Dual-mode upconversion nanoprobe enables broad-range thermometry from cryogenic to room temperature. *ACS Appl. Mater. Interfaces* **2019**, *11*, 42455−42461.

(2) Jaque, D.; Vetrone, F. Luminescence nanothermometry. *Nanoscale* **2012**, *4*, 4301−4326.

(3) Runowski, M.; Bartkowiak, A.; Majewska, M.; Martín, I. R.; Lis, S. Upconverting lanthanide doped fluoride $NaLuF_4$: Yb^{3+}-Er^{3+}-Ho^{3+}-optical sensor for multi-range fluorescence intensity ratio(FIR) thermometry in visible and NIR regions. *J. Lumin.* **2018**, *201*, 104−109.

(4) Li, D.; Wang, Y.; Zhang, X.; Yang, K.; Liu, L.; Song, Y. Optical temperature sensor through infrared excited blue upconversion emission in Tm^{3+}/Yb^{3+} co-doped Y_2O_3. *Opt. Commun.* **2012**, *285*, 1925−1928.

(5) Brites, C. D. S.; Balabhadra, S.; Carlos, L. D. Lanthanide-based thermometers: At the cutting-edge of luminescence thermometry. *Adv. Opt. Mater.* **2019**, *7*, 1801239.

(6) Tu, X.; Xu, J.; Li, M.; Xie, T.; Lei, R.; Wang, H.; Xu, S. Color-tunable upconversion luminescence and temperature sensing behavior of Tm^{3+}/Yb^{3+} codoped $Y_2Ti_2O_7$ phosphors. *Mater. Res. Bull.* **2019**, *112*, 77−83.

(7) Dong, B.; Cao, B.; He, Y.; Liu, Z.; Li, Z.; Feng, Z. Temperature sensing and in vivo imaging by molybdenum sensitized visible upconversion luminescence of rare-earth oxides. *Adv. Mater.* **2012**, *24*, 1987−1993.

(8) Stem, M. R. Photon−phonon anti-stokes upconversion of a photonically, electronically, and thermally isolated opal. *Appl. Phys. B: Lasers Opt.* **2016**, *122*, 113.

(9) Vetrone, F.; Boyer, J. C.; Capobianco, J. A.; et al. Effect of Yb^{3+} co-doping on the upconversion emission in nanocrystalline Y_2O_3: Er^{3+}. *J. Phys. Chem. B* **2003**, *107*, 1107−1112.

(10) Fischer, L. H.; Harms, G. S.; Wolfbeis, O. S. Upconverting nanoparticles for nanoscale thermometry. *Angew. Chem., Int. Ed.* **2011**, *50*, 4546−4551.

(11) Wang, Y.; Lei, L.; Ye, R.; Jia, G.; Hua, Y.; Deng, D.; Xu, S. Integrating positive and negative thermal quenching effect for ultrasensitive ratiometric temperature sensing and anti-counterfeiting. *ACS Appl. Mater. Interfaces* **2021**, *13*, 23951−23959.

(12) Runowski, M.; Shyichuk, A.; Tyminski, A.; Grzyb, T.; Lavín, V.; Lis, S. Multifunctional optical sensors for nanomanometry and nanothermometry: High-pressure and high-temperature upconversion luminescence of lanthanide-doped phosphates-$LaPO_4$/YPO_4:Yb^{3+}-Tm^{3+}. *ACS Appl. Mater. Interfaces* **2018**, *10*, 17269−17279.

(13) Casagrande, E.; Back, M.; Cristofori, D.; Ueda, J.; Tanabe, S.; Palazzolo, S.; Rizzolio, F.; Canzonieri, V.; Trave, E.; Riello, P. Upconversion-mediated boltzmann thermometry in double-layered Bi_2SiO_5:Yb^{3+}, Tm^{3+}@SiO_2 hollow nanoparticles. *J. Mater. Chem. C* **2020**, *8*, 7828−7836.

(14) Liu, J.; Deun, R.; Kaczmarek, A. Eu^{3+}, Tb^{3+}- and Er^{3+}, Yb^{3+}-doped α-MoO_3 nanosheets for optical luminescent thermometry. *Nanomaterials* **2019**, *9*, 646.

(15) Lei, L.; Liu, E.; Wang, Y.; Hua, Y.; Zhang, J.; Chen, J.; Mao, R.; Jia, G.; Xu, S. Amplifying upconversion by engineering interfacial density of state in sub-10 nm colloidal core/shell fluoride nanoparticles. *Nano Lett.* **2021**, *21*, 10222−10229.
(16) Xu, W.; Lei, L.; Wang, Y.; Liu, E.; Chen, L.; Xu, S. Modulating electron population pathways for time-dependent dynamic multicolor displays. *Mater. Horiz.* **2021**, *8*, 3443−3448.
(17) Meza, O.; Diaz-Torres, L. A.; Salas, P.; Rosa, E.; Solis, D. Color tunability of the upconversion emission in Er-Yb doped the wide band gap nanophosphors ZrO_2 and Y_2O_3. *Mater. Sci. Eng., B* **2010**, *174*, 177−181.
(18) Diaz-Torres, L. A.; Meza, O.; Solis, D.; Salas, P.; Rosa, E. Visible upconversion emission and non-radiative direct Yb^{3+} to Er^{3+} energy transfer processes in nanocrystalline ZrO_2:Yb^{3+},Er^{3+}. *Opt. Lasers Eng.* **2011**, *49*, 703−708.
(19) Kumar, K. U.; Vijaya, N.; Oliva, J.; Jacinto, C.; Rosa, E.; Jayasankar, C. Multicolor upconversion emission and color tunability in Tm^{3+}/Er^{3+}/Yb^{3+} tri-doped $NaNbO_3$ nanocrystals. *Mater. Express* **2012**, *2*, 294−302.
(20) Rakov, N.; Gómez, L. A.; Rátiva, D. J.; Maciel, G. S. Blue upconversion emission from Tm^{3+} sensitized by Nd^{3+} in aluminum oxide crystalline ceramic powders. *Appl. Phys. B: Lasers Opt.* **2009**, *94*, 199−202.
(21) Li, H.; Sun, X.; Muhammad, K. S.; Liu, L. Commendable Pr^{3+}-activated $Ba_2Ga_2GeO_7$ phosphor with high-brightness white long-persistent luminescence. *J. Mater. Chem. C* **2019**, *7*, 7984.
(22) Chen, G.; Lei, R.; Huang, F.; Wang, H.; Zhao, S.; Xu, S. Effects of Tm^{3+} concentration on upconversion luminescence and temperature-sensing behavior in Tm^{3+}/Yb^{3+}:Y_2O_3 nanocrystals. *Luminescence* **2018**, *33*, 1262−1267.
(23) Li, Y.; Li, Y. M.; Zhou, J.; Zheng; Wang, R. Upconversion luminescence, and temperature sensing properties of $12CaO{\cdot}7Al_2O_3$ single crystal sensitized with lanthanide ions Er(III) and Yb(III). *Talanta* **2020**, *207*, No. 120292.
(24) Hayashi, K.; Matsuishi, S.; Ueda, N.; Hirano, M.; Hosono, H. Maximum incorporation of oxygen radicals, O^- and O^{2-}, into $12CaO{\cdot}7Al_2O_3$ with a nanoporous structure. *Chem. Mater.* **2003**, *15*, 1851−1854.
(25) Yanagi, H.; Kuroda, T.; Kim, K. B.; Toda, Y.; Hosono, H. Electron injection barriers between air-stable electride with low work function, C12A7:e^-, and pentacene, C60 and copper phthalocyanine. *J. Mater. Chem.* **2012**, *22*, 4278−4281.
(26) Sushko, P. V.; Shluger, A. L.; Hayashi, K.; Hirano, M.; Hosono, H. Hopping and optical absorption of electrons in nano-porous crystal $12CaO{\cdot}7Al_2O_3$. *Thin Solid Films* **2003**, *445*, 161−167.
(27) Hayashi, K.; Hirano, M.; Hosono, H. Thermodynamics and kinetics of hydroxide ion formation in $12CaO{\cdot}7Al_2O_3$. *J. Phys. Chem. B* **2005**, *109*, 11900−11906.
(28) Wang, Z.; He, X.; Yong, T. Y.; Miao, Y.; Zhang, C.; Tang, B. Z. Multicolor tunable polymeric nanoparticle from tetraphenylethylene cage for temperature sensing in living cells. *J. Am. Chem. Soc.* **2020**, *142*, 512−519.

https://doi.org/10.1021/acsomega.3c01372
ACS Omega 2023, 8, 15730−15740